RADIO EMISSION FROM THE SUPERNOVA REMNANT VELA-X

By D. K. Milne*

Summary

Radio observations are presented of the fairly large galactic complex Vela-X, Y, and Z. These sources are believed to be the remnant of a supernova having an optical identification with the filamentary nebula Stromlo 16. The brightness distributions, obtained at four frequencies, indicate an open annular structure reminiscent of other supernova remnants. The variation of spectral index over the region is investigated and shows that the radiation is substantially nonthermal, the integrated fluxes yielding a spectral index of $-0\cdot3$. A high resolution distribution of magnetic field direction is deduced from polarization measurements made at three frequencies; a circumferential magnetic field is a possible interpretation of the field orientations.

I. Introduction

Up to the present time, radio emission has been detected from some 20 objects believed to be the remnants of galactic supernovae. Most of these objects are characterized at radio frequencies by a nonthermal spectral index and by a structure suggesting that the emission arises predominantly from the outer envelope of the expanding gas volume. Radio polarization has been detected from very few of these objects—many are of small angular dimensions or low surface brightness, making detailed observations difficult.

One of the largest and brightest objects believed to be of supernova origin is the complex of radio sources known as Vela-X, Y, and Z. Its area is about 8 square degrees and its flux density greater than 1000 f.u.† at decimetre wavelengths. It is believed that this complex is the remnant of a supernova having an optical identification with the filamentary nebulosity Stromlo 16 (Gum 1955).

Little attention has been given to this southern object. It appears as part of an isolated region (the Vela–Puppis complex) in the galactic surveys of Piddington and Trent (1956), Hill, Slee, and Mills (1958), Wilson and Bolton (1960), and Mathewson, Healey, and Rome (1962). The only detailed radio study of this region was made by Rishbeth (1958) with the Mills Cross instruments at 85 MHz ($0°\cdot8$ beamwidth) and 19·6 MHz ($1°\cdot2$ beamwidth). The three sources Vela-X, Y, and Z can be distinguished in his 85 MHz isotherms but are not resolved at 19·6 MHz. Rishbeth concluded that the three sources were all of a nonthermal character, with Vela-X possibly having a flatter spectral index than the other two. Rishbeth decided against the identification of Vela-X with Stromlo 16 on the grounds that the

radio brightness distribution was of smaller extent than that outlined by Stromlo 16 and that the peak radio emission was in an area devoid of filaments. The first proposal of the supernova origin of these radio sources was by Wilson and Bolton (1960), who from their 960 MHz galactic survey concluded that Vela-X, Y, and Z were portions of the one source, a supernova associated with Stromlo 16. Harris (1962) included Vela-X, Y, and Z in his evolutionary studies of supernova remnants. He arrived at estimated distances of 460 pc by Shklovsky's radio method and 700 pc from the angular dimensions of individual filaments. Harris adopted a flat spectral index ($a = 0 \cdot 00 \pm 0 \cdot 15$) from the 85 MHz results of Rishbeth and the 960 MHz results of Wilson and Bolton.

Mathewson, Healey, and Rome (1962), from their 1440 MHz survey, showed that Vela-X had a thermal spectrum and Vela-Y a nonthermal spectrum. Linear polarization in the brightest region of Vela-X has been reported at 1410 MHz by Gardner and Whiteoak (1962), showing that Vela-X is not entirely thermal. Optical spectra have been obtained for two of the filaments in Stromlo 16 (Milne 1968). Indications are of the presence of collisionally excited gas, probably associated with shock fronts.

The results reported here are of radio surveys of the Vela complex carried out by the author between March 1963 and April 1966. From these results it would appear that Vela-X, Y, and Z is a supernova remnant having a reasonably well-defined magnetic field and a positive identification with the filamentary nebula Stromlo 16.

II. RADIO OBSERVATIONS

The 210 ft radio telescope of the Australian National Radio Astronomy Observatory at Parkes, N.S.W., was used to map the intensity and polarization of the continuum radio emission from the Vela complex. The surveys were carried out

TABLE 1

DETAILS OF RECEIVING SYSTEM

Centre Frequency (MHz)	Bandwidth (MHz)	System Noise Temp. (°K)	Beamwidth (min arc)	Assumed Flux Densities of Calibrating Sources (f.u.)	
				Hydra A	04−71
408	8	350	48	135	40
635	8	180	31	91	Not used
1410	10	100	14·1	42	13·5
1660	10	400	12·6	36	Not used
2650	50	180	7·5	23·5	7·5

using a 408 MHz double sideband crystal-mixer receiver (described by Mackey 1964), a 635 MHz nondegenerate parametric receiver (Ferranti model VCA/L10), a 1410 MHz degenerate parametric receiver (Gardner and Milne 1963), a 1660 MHz crystal-mixer receiver, and a 2650 MHz degenerate parametric receiver (Cooper, Cousins, and Gruner 1964). Details of the receiver–antenna performance at each frequency are given in Table 1. Nightly calibration of the receiver–antenna system was made
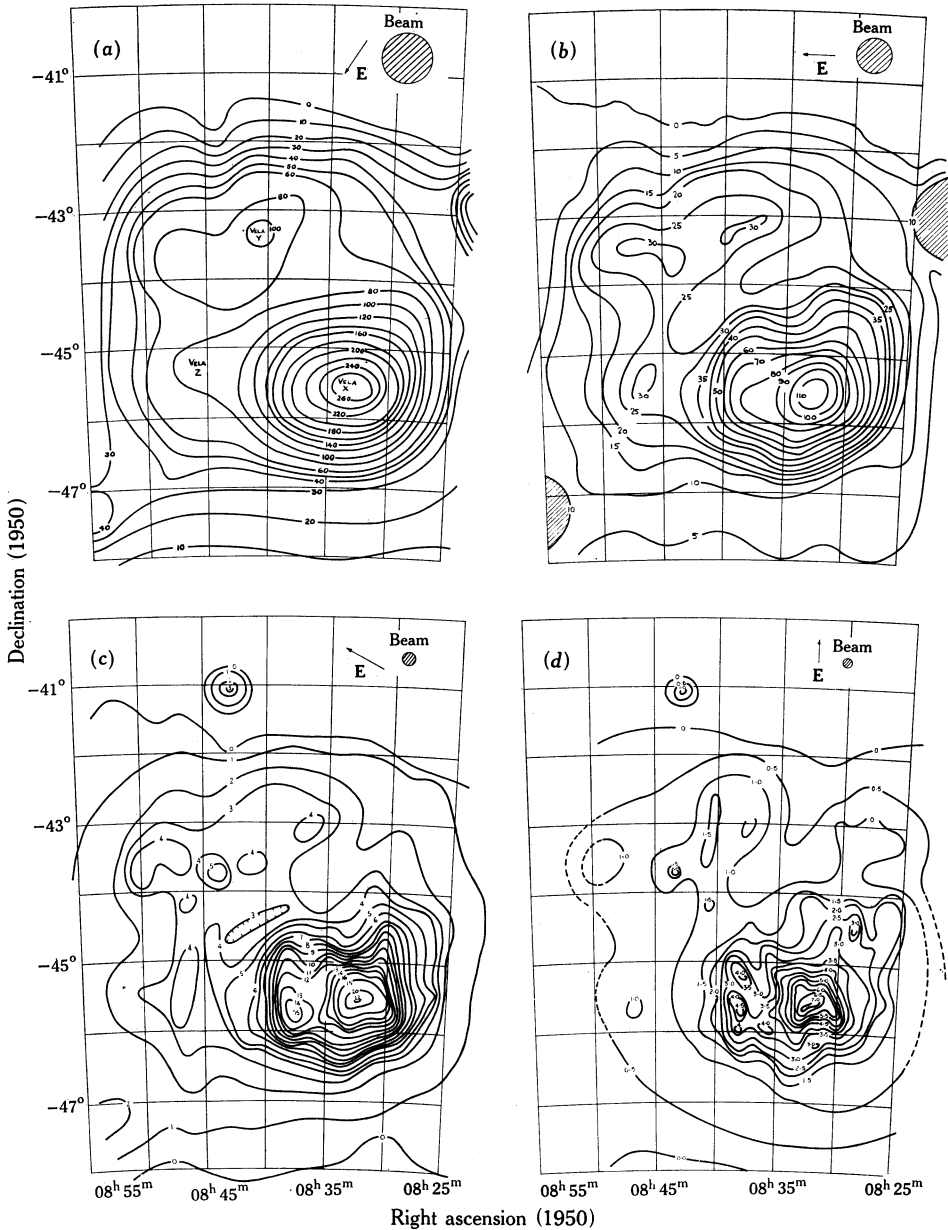
Fig. 1.—Isotherms of brightness temperature at (a) 408, (b) 635, (c) 1410, and (d) 2650 MHz. The respective directions of the electric vector of the aerial feed are shown on each figure. For (a) at the frequency of 408 MHz the beamwidth of the 210 ft telescope is comparable with that used by certain earlier workers. This figure shows the three sources Vela-X, Y, and Z into which these observers resolved the region.

using the radio sources Hydra A or MSH 04—71. An argon discharge noise generator was used to interpolate equipment performance between these observations.

The brightness temperatures T_b quoted here were derived at each frequency from the relationship

$$T_b = \lambda^2 S / 2k(1 \cdot 13\,B^2),$$

where k is Boltzmann's constant ($1 \cdot 38 \times 10^{-23}$ J degK^{-1}), λ is the wavelength (metres), and B is the half-power width (radians) of the antenna response to a point source of known flux S (f.u.). This relationship is valid for a Gaussian antenna response, the solid angle of the beam being given by $1 \cdot 13\,B^2$ under this condition. Scans were made over Hydra A from which values of B and peak deflection were obtained. The flux densities adopted for Hydra A and 04—71 at each frequency are given in Table 1.

(a) Continuum Surveys

A region amounting to some 40 square degrees around Vela-X was mapped, in one polarization, at frequencies of 408, 635, 1410, and 2650 MHz. These surveys were carried out using declination scans spaced by approximately half-beamwidth intervals in right ascension. The feed angle was changed slightly between scans to keep the average position angle of polarization approximately constant throughout the observations. Drive rates in declination were chosen such that about eight time constants were contained in each beamwidth. These scans were combined with right ascension scans through the regions of lower intensity to the north and south of the brighter complex. Isotherms of brightness temperature drawn from these scans appear in Figures 1(a)–1(d). The isotherms are accurate to within half a contour unit for the polarization chosen. The baselevels over which they are drawn are arbitrary.

(b) Polarization Surveys

These investigations were carried out over most of the complex at frequencies of 1410 and 2650 MHz. The region was sampled at 408 MHz but no significant polarization was found at this frequency. It was necessary to provide observations at a third frequency to remove ambiguities of integral multiples of π from the Faraday rotation between 1410 and 2650 MHz. The 1660 MHz observations, at selected points in the region, were used for this purpose. In addition, two regions near R.A. 08^{h}36^m, Dec. —45° and R.A. 08^{h}31^m, Dec. —46° (1965), showing strong uniform polarization at these three frequencies, were observed with the 1660 MHz receiver detuned by ±30 MHz to 1630 and 1690 MHz.

The basic procedure that was followed for the polarization measurements was to rotate the feed on the telescope at 180 deg/min at each of a series of grid points over the region. This, in principle, would contain a sinusoidal modulation of period 180° (in feed angle). The amplitude of this would be proportional to the linearly polarized component of the continuum emission. The feed angle of maximum emission gives, after correcting for parallactic angle, the position angle of the electric

vector of the emission. In practice, however, there are two classes of spurious effects that must be removed from the observations. These are due to:

(1) Ground reflection and emission. This effect, being a function of telescope position relative to the ground, can be removed by comparing the modulation on the source with that off the source at the same altitude–azimuth position.

(2) Beam ellipticity and squint. These effects depend on the brightness gradient at the point of observation. They were assessed on a strong source each observing run and found to be negligible for the fairly shallow brightness gradients in the Vela-X region.
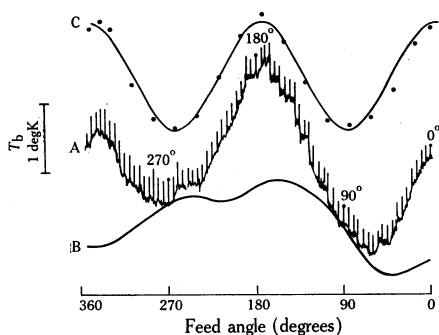

Fig. 2.—Tracing of a record used to determine the polarization at a point in the nebula showing (A) the receiver output when the aerial feed is rotated with the antenna pointed at a strongly polarized point in the region; (B) the receiver output when the feed is rotated on the unpolarized background, in this case the average of rotations on several unpolarized points; and (C) the difference between (A) and (B) showing the sinusoidal modulation from which the magnitude and feed angle of the polarized component is measured.

For a detailed discussion of these spurious effects, and their removal in the analysis, the reader is referred to Gardner and Davies (1966). A sample record of the receiver output during feed rotations on a strongly polarized region and on the background is shown in Figure 2. The resultant modulation obtained by subtracting the modulation on the background from that on the source is also shown.

In addition to the measurements described, scans were made over selected regions with polarization position angles spaced at intervals of 30°. These measurements provided an independent check on the main method used and gave additional information on the distribution of polarization over these regions.

The results of the polarization measurements are presented in Figure 3 and Table 2.

(i) *Figure 3*

The magnitudes and directions of the electric vectors, measured at all the sky positions investigated, are plotted in equatorial coordinates (1950 epoch) in Figures 3(a)–3(c) for 1410, 1660, and 2650 MHz respectively. The E vector position angle and magnitude are shown in the usual convention—the thicker the vector the more reliable the observation.
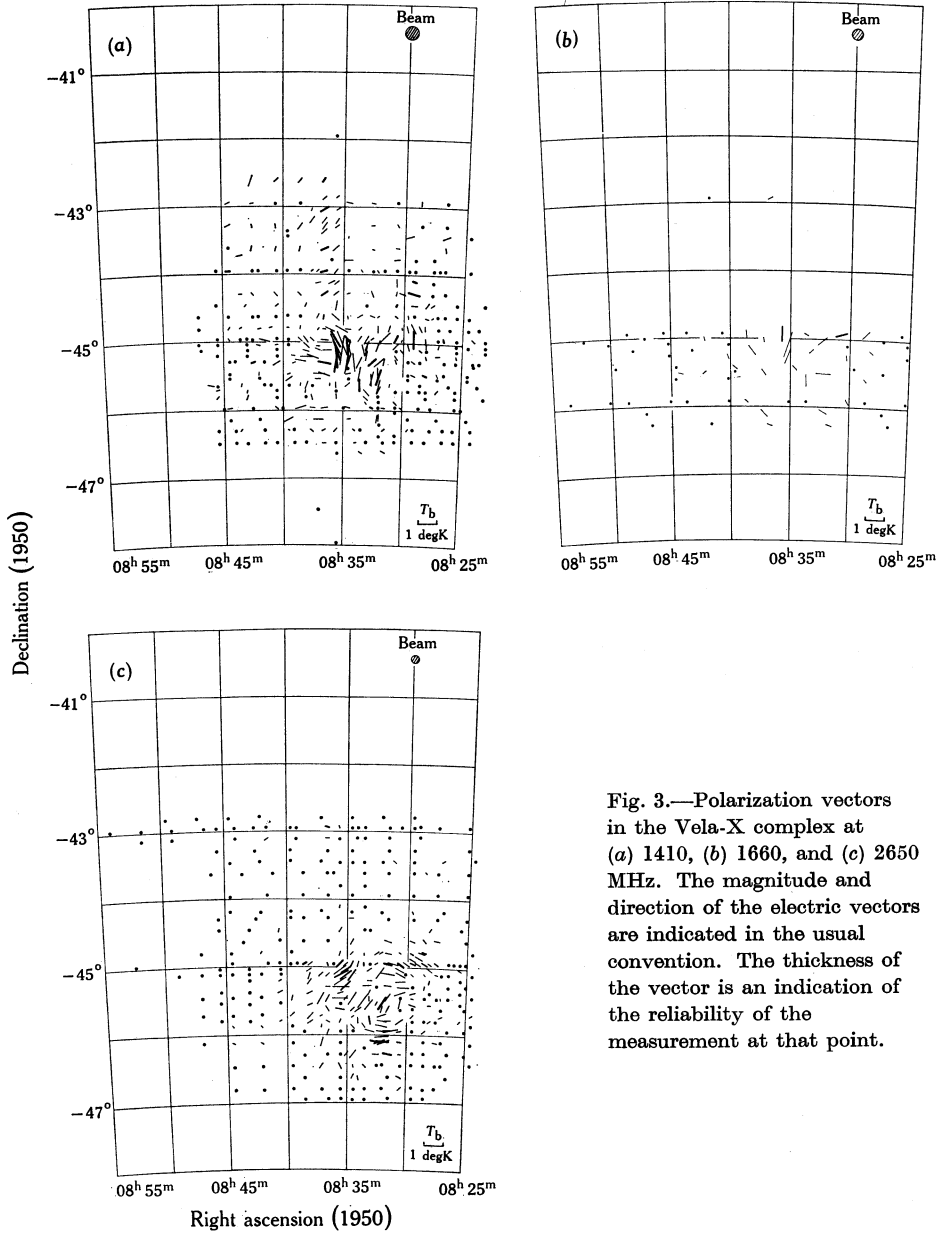
Fig. 3.—Polarization vectors in the Vela-X complex at (a) 1410, (b) 1660, and (c) 2650 MHz. The magnitude and direction of the electric vectors are indicated in the usual convention. The thickness of the vector is an indication of the reliability of the measurement at that point.

(ii) *Table 2*

Space does not permit the inclusion in tabular form of all the polarization results.* Table 2 is therefore limited to those sky positions where there are sufficient data to derive the directions of the intrinsic polarization, in accordance with Section IV. The notation used in Table 2 to specify the polarization is: the electric vector position angle (degrees); polarization brightness temperature, $\frac{1}{2}$(maximum — minimum) (degK). The number of independent observations made is given in parentheses (only one observation is implied when this is omitted). The equatorial positions quoted are those at which the observations were made ($\sim 1965 \cdot 0$).

TABLE 2

POLARIZATION RESULTS

The number of independent observations (when more than one was made) is given in parentheses

Position (1965)				Posn. Angle (deg); Pol. Temp. (°K) for Frequency (MHz) of:			Intrinsic Position Angle °	Rotation Measure (rad/m²)	Polarization Ratio
R.A.			Dec.						
h	m	s	°	′	1410	1660	2650			
08	27	30	−45	30	24; 0·2		17; 0·2(2)	12	+7	2·3
08	27	30	−45	45	144; 0·3		117; 0·2	106	+15	1·5
08	28	00	−44	40	138; 0·15		79; 0·35	54	+34	6·2
08	28	30	−44	30	144; 0·35		151; 0·15	85	+90	1·0
08	28	30	−45	00	0; 0·2		59; 0·3	10	+67	4·0
08	28	30	−45	05	178; 0·2		55; 0·4	10	+61	5·3
08	28	30	−45	15	17; 0·2	49; 0·2	164; 0·3	100	+64	3·4
08	29	00	−44	50	26; 0·4		69; 0·35(3)	16	+59	2·6
08	29	00	−45	00		136; 0·5	58; 0·4(2)	5	+72	
08	29	00	−45	10	59; 0·2		49; 0·2(2)	45	+5	2·4
08	29	30	−45	00	179; 1·0(3)		59; 0·4(4)	10	+67	1·3
08	30	00	−44	40	10; 0·2		75; 0·35(2)	30	+57	5·5
08	30	00	−44	50	19; 0·4		60; 0·3(2)	0	+82	2·8
08	30	00	−45	00	161; 0·2		57; 0·4	10	+64	6·6
08	30	30	−45	20		12; 0·3	90; 0·4	73	+17	
08	30	30	−46	00	65; 0·2	29; 0·3		115	+35	
08	31	00	−45	00	145; 0·45(2)	108; 0·6(2)	56; 0·45(3)	20	+49	3·5
08	31	00	−45	05	55; 0·2(2)		60; 0·65	30	+41	11·0
08	31	00	−45	15	33; 0·35		93; 0·5	45	+65	4·8
08	31	00	−45	20	29; 0·35		83; 0·35	36	+64	3·3
08	31	00	−46	00	61; 0·2		106; 0·3	55	+69	5·0
08	32	00	−45	00	139; 0·85		77; 0·5(2)	52	+34	2·0
08	32	00	−45	20	170; 0·35		85; 0·45	50	+48	3·7
08	32	00	−46	00	82; 0·3		92; 0·4(2)	30	+84	4·3
08	32	00	−46	20	134; 0·2	110; 0·3	80; 0·5(4)	60	+27	6·6
08	32	00	−46	30	Nil		78; 0·3 ⎫	84	−8	
08	32	00	−46	40	61; 0·3		Nil ⎬			
08	32	24	−45	34	164; 0·8(15)	88; 0·8	150; 0·8	70	+109	3·1
08	32	30	−44	50	0; 0·4		116; 0·3	111	+7	
08	32	30	−45	05	159; 0·65	129; 0·6	98; 0·5(2)	74	+24	11·0
08	32	30	−45	40	173; 0·75(2)		162; 0·4	90	+98	1·6
08	32	30	−45	45	157; 0·7		114; 0·5	100	+19	2·2
08	32	30	−46	08	177; 0·4		112; 0·5	16	+130	4·4
08	32	30	−46	10	172; 0·45	61; 0·4	90; 0·8(6)	171	+135	7·0
08	33	00	−45	00	126; 0·2(2)		125; 0·2(2)	125	0	3·1
08	33	00	−45	34	158; 0·65		154; 0·3	80	+100	1·4
08	33	30	−45	05	161; 0·5		130; 0·15	120	+14	1·0
08	33	30	−45	10	166; 0·5		120; 0·35(2)	100	+27	2·4
08	33	30	−45	15		132; 0·3	91; 0·3	65	+35	

* Complete results of the polarization measurements are available in tabular form on request to the Chief, Division of Radiophysics, CSIRO, Box 76, P.O. Epping, N.S.W. 2121.

TABLE 2 (*Continued*)

Position (1965)			Posn. Angle (deg); Pol. Temp. (°K) for Frequency (MHz) of:			Intrinsic Position Angle	Rotation Measure	Polarization Ratio
R.A.		Dec.	1410	1660	2650	°	(rad/m²)	
h m s	°	′						
08 33 30	−45	50	48; 0·35		8; 0·5(2)	173	+20	4·1
08 33 30	−45	55	31; 0·2			20	+74	9·0
08 33 30	−46	00			74; 0·5			
08 34 00	−44	50	133; 0·2		4; 0·15(2)	135	+67	2·5
08 34 00	−45	00	144; 0·35	61; 0·2	4; 0·3(4)	134	+68	2·7
08 34 00	−45	30	169; 0·8		145; 1·05	135	+13	4·2
08 34 00	−45	40	0; 0·65(3)	0; 0·6	148; 0·8	134	+19	4·0
08 35 00	−44	20	107; 0·15		95; 0·3	90	+7	4·5
08 35 00	−44	40	25; 0·2		151; 0·3	131	+27	5·0
08 35 00	−44	50	85; 0·35		140; 0·3	90	+67	3·0
08 35 00	−45	00	47; 0·5(2)		154; 0·35(3)	124	+41	2·6
08 35 00	−45	10	179; 1·4		145; 0·75(2)	132	+18	1·7
08 35 00	−45	30	100; 0·35	43; 0·35	147; 0·8	93	+74	7·7
08 35 00	−45	40	132; 0·35		137; 0·35	139	−3	3·3
08 35 00	−46	10	102; 0·2		169; 0·15	124	+60	2·4
08 35 30	−45	05	23; 1·4		128; 0·65(2)	95	+45	1·6
08 35 30	−45	10	177; 1·6	162; 1·4	128; 0·8(2)	108	+27	1·6
08 35 30	−45	20		159; 0·9	133; 0·75(2)	115	+24	
08 36 00	−42	55	132; 0·2					
08 36 00	−43	00			27; 0·15	170	+50	3·7
08 36 00	−43	05	125; 0·3					
08 36 00	−44	00	141; 0·35					
08 36 00	−44	10			170; 0·15	116	+74	1·2
08 36 00	−44	20	130; 0·35					
08 36 00	−44	30	169; 0·5		155; 0·3	149	+8	1·8
08 36 00	−45	00	32; 1·0(10)	178; 0·8(2)	136; 0·5(10)	108	+38	1·5
08 36 00	−45	05	30; 0·135		126; 0·85	91	+48	2·1
08 36 00	−45	10	15; 1·2(2)		120; 0·85(2)	91	+40	2·6
08 36 00	−45	15	7; 1·1(2)		124; 0·8	100	+33	2·8
08 36 00	−45	20	169; 1·25(2)		90; 0·85	73	+23	2·8
08 36 00	−45	40	5; 0·35		80; 0·5	40	+54	4·7
08 36 00	−45	50	5; 0·3		159; 0·3(2)	150	+12	3·3
08 37 00	−43	00		114; 0·3	70; 0·35(3)	48	+30	
08 37 00	−43	05	128; 0·3(4)					
08 37 00	−43	10			92; 0·2	75	+23	2·0
08 37 00	−43	15	141; 0·4					
08 37 00	−45	00	85; 0·4		23; 0·2(3)	112	+123	2·2
08 37 00	−45	10	92; 0·45		135; 0·35	80	+55	3·2
08 37 00	−45	20	78; 0·75(2)		90; 0·3	120	+48	1·7
08 37 00	−45	30	71; 0·65		155; 0·45	115	+40	2·6
08 37 00	−46	00	110; 0·4		160; 0·35	108	+71	3·1
08 37 00	−46	20	117; 0·2	69; 0·3	Nil	120	+68	
08 37 30	−45	05	90; 0·2	12; 0·25		85	+54	5·5
08 37 30	−45	10	69; 0·3		135; 0·5			
08 37 30	−45	30	87; 0·5		151; 0·75	110	+56	2·7
08 37 30	−45	34	93; 0·35	36; 0·35	168; 0·3	130	+52	3·6
08 37 30	−46	10	92; 0·5	42; 0·55	168; 0·5	130	+52	3·7
08 38 30	−45	00	39; 0·45		132; 0·3	100	+44	2·6
08 38 30	−45	05	45; 0·4		123; 0·35	85	+52	2·8
08 38 30	−45	10	76; 0·4		160; 0·4	125	+48	2·9
08 38 30	−45	15	90; 0·6	38; 0·6	150; 0·65	95	+75	3·2
08 38 30	−45	45	171; 0·4		143; 0·4	132	+15	5·9
08 39 00	−45	00	47; 0·35	6; 0·4	126; 0·3(2)	88	+52	2·8
08 40 00	−45	30	112; 0·2	49; 0·3	163; 0·35	115	+65	6·6
08 40 00	−46	10	118; 0·5		13; 0·15	155	+52	11·0
08 41 00	−44	30	132; 0·2		163; 0·2	103	+82	2·5
08 41 00	−45	15	Nil		128; 0·2			
08 41 00	−45	20	107; 0·5			65	+82	1·4
08 41 00	−45	25			121; 0·2			
08 42 30	−44	50	105; 0·2		157; 0·2	105	+71	3·1
08 42 30	−45	05	75; 0·4	14; 0·2		40	+54	
08 45 00	−44	50	157; 0·2		170; 0·15	110	+82	7·7

Coordinates of these points for the 1950 epoch are approximately given by the addition of $-0^m \cdot 5$ and $+3'$ to the right ascension and declination respectively.

III. RADIO SPECTRAL INDEX

Basically two determinations for the relationship between brightness temperature (or flux) and frequency are available. The first of these, yielding "the spatial distribution of spectral index", compares brightness distributions at different frequencies but with the same resolution. This can be accomplished by convolving high resolution maps with a function designed to degrade the resolution to that of a lower resolution survey. This comparison can be made directly if brightness distributions are available at the same resolution. The second method, producing "the total integrated spectral index", is to integrate the brightness contours obtained for the source at each frequency and to fit a relationship of the form $S \propto f^a$ to these integrated fluxes.
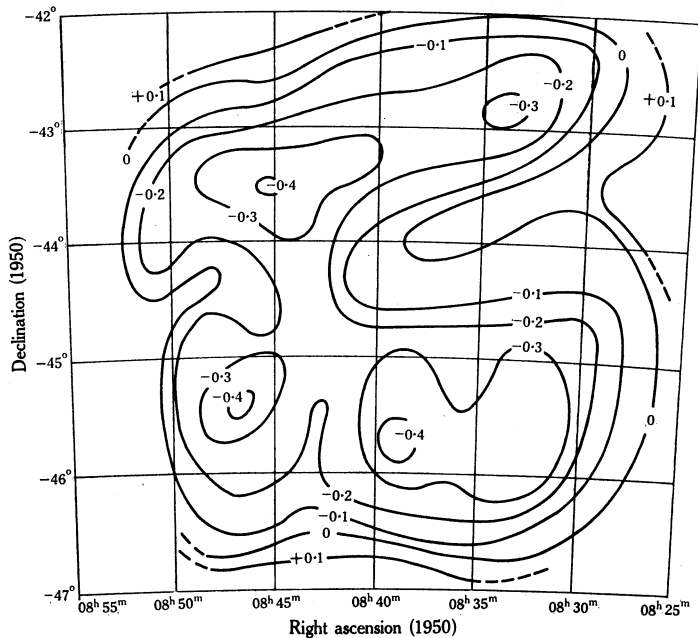
Fig. 4.—Contours of spectral index a in the Vela-X region. These contours were constructed from a comparison of the 635 MHz isotherms (Fig. 1(b)) with the 1410 and 2650 MHz isotherms (Figs. 1(c) and 1(d)) degraded in resolution to 31' arc.

(a) Spatial Distribution of Spectral Index

Four brightness distributions, at a comparable resolution, are available for the Vela region: the surveys of Rishbeth (1958) at 85 MHz, Wilson and Bolton (1960) at 960 MHz, Mathewson, Healey, and Rome (1962) at 1440 MHz, and the present survey at 408 MHz—with beamwidths of $0° \cdot 8$, $0° \cdot 8$, 50', and 48' respectively. Three points in the region were compared for these four surveys, yielding values of a

in the relation $T_{\mathrm{b}} \propto f^{a-2}$ of $-0\cdot3\pm0\cdot2$ for Vela-X and $-0\cdot6\pm0\cdot4$ for both Vela-Y and Z.

The distribution of spectral index was also investigated at two higher resolutions. Using the CDC 3600 computer of CSIRO the 2650 and 1410 MHz brightness distributions were convolved (Figs. 1(d) and 1(c)) with functions designed to degrade these $7'\cdot5$ and $14'\cdot1$ beamwidths to $3'\cdot0$, the beamwidth of the 635 MHz map. A comparison was then made between the degraded 2650 and 1410 MHz brightness isotherms and the observed isotherms at 635 MHz, resulting in the distribution of spectral index

TABLE 3

INTEGRATED FLUXES FOR VELA-X, Y, AND Z

Frequency (MHz)	Integrated Flux (f.u.)	Reference
19	960	Rishbeth (1958)
86	2900 ± 1000*	Rishbeth (1958)
408	$2300\pm\ 300$	Present result
635	$2360\pm\ 300$	Present result
960	1560	Harris (1962)
1410	$1640\pm\ 300$	Present result
1440	1610*	Mathewson, Healey, and Rome (1962)
2650	$1400\pm\ 250$	Present result

* Rishbeth (1958) and Mathewson, Healey, and Rome (1962) give integrated fluxes for Vela-X only. The values given above include Vela-Y and Z and have been obtained by integrating the previous workers' isotherms. It was not considered necessary to estimate errors for the 1440 MHz point; it is very close to the value measured at 1410 MHz in the present paper.

shown in Figure 4. There is good agreement in the contour shape between the three maps of equal resolution, with most of the differences resulting from what is apparently a thermal region centred at R.A. $08^{\mathrm{h}}\,35^{\mathrm{m}}$, Dec. $-44°$ and a steepening of the spectrum (more nonthermal) over the eastern side and a nonthermal region near R.A. $08^{\mathrm{h}}\,34^{\mathrm{m}}$, Dec. $-43°$. This latter area is of low surface brightness and the steepness of its spectrum is questionable, although we see in Section IV that there is an isolated patch of polarization close to this position. Over the bulk of Vela-X the spectral index a was found to be about $-0\cdot3$ with values of $-0\cdot35$ on the peak of Vela-X and $-0\cdot4$ near Vela-Y and Z. The positive values of a around the periphery of the source are not significant; the errors are large here and the baselevels of the three surveys used are not absolutely determined.

(b) *Total Integrated Spectrum*

Integrated fluxes* have been obtained for the surveys described here and are shown in Table 3, together with estimates made by other workers. The variation of integrated flux with frequency is displayed in Figure 5. The power-law spectrum of best fit is indicated; the spectral index is in this case $-0\cdot3\pm0\cdot1$ and applies to the whole region Vela-X, Y, and Z.

* These fluxes are revised values of those given in Milne (1966); both sets lie within the estimated errors.

All these spectral indices confirm earlier suggestions that the region is non-thermal, with Vela-Y and Z having steeper radio spectra than Vela-X (Rishbeth 1958). There is the possibility of considerable free–free radio emission from this region; this is evident from the presence of Hα emission and the fairly flat spectral index. The magnitude of this thermal component could be estimated if observations were made at a frequency high enough to observe a flattening of the spectral index when the flux of the nonthermal component falls to well below that of the thermal part. This flattening is not evident in Figure 5.
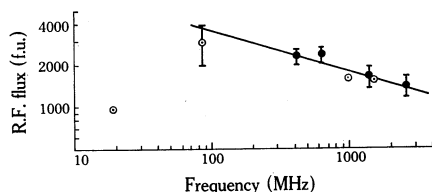
Fig. 5.—Integrated radiofrequency spectrum of Vela-X, Y, and Z. The data used in this figure are taken from Table 3. The full circles represent the present flux determinations. The line shown is for a spectral index of −0·3.

Estimates of free–free radio emission made from the Hα flux are discussed in Section VII.

IV. RADIO POLARIZATION AND DIRECTIONS OF MAGNETIC FIELD

An important feature of the radio emission from this complex is the considerable degree of linear polarization detected over much of the region. With polarization greater than 20%, this source is one of the most highly polarized galactic objects known. The distributions over the source of the magnitude and direction of the polarization at 1410, 1660, and 2650 MHz are shown in the vector presentations of Figures 3(a)–3(c). The percentage polarization, which is not given in the diagrams but can be gauged at 1410 and 2650 MHz by comparing Figures 3(a) and 1(c) or Figures 3(c) and 1(d), is greatest around the periphery of the principal source (Vela-X). At 2650 MHz the polarization is in excess of 20% in three substantial regions centred on R.A. $08^h 30^m$, Dec. −45°; $08^h 35^m$, −45°10′; and $08^h 32^m \cdot 5$, −46°. Weaker polarization extends over the region to the east occupied by Vela-Y and Z, whilst the peak of Vela-X is polarized at a lower percentage polarization than the surrounding region. Most of the outlying parts examined for polarization yielded magnitudes of T_b less than 0·1°K, the lower limit of the survey. The presence of polarization near R.A. $08^h 36^m$, Dec. −43° is, however, worth noting. There is a steepening of the spectral index close to this position (Fig. 4).

Intrinsic directions of polarization obtained over most of the source are given in Table 2, together with the rotation measures at these points. The derivation of these followed a simple graphical fit of the position angles at each frequency to a λ^2 law (i.e. Faraday rotation). The lowest values for the rotation measure consistent with the data were the ones accepted. No corrections for ionospheric Faraday rotation were made to the values of Table 2. For these observations, made at night near sunspot minima, the errors introduced by neglecting this can be no more than 2° at 1410 MHz, and less than 1° at 2650 MHz.

An expression for the error in the magnitude of the polarization, introduced by the finite bandwidth of the receiving system, is given by Gardner and Whiteoak

(1966). With the bandwidths used here and the rotation measures detected it is clear that no correction need be made for this effect. It is thought that the error in a single observation is $\pm10°$ in position angle and $\pm0\cdot1$ degK in magnitude. This conclusion was reached from an analysis of the sets of independent observations made on certain sky positions. This would lead to an error of $\pm20°$ in the position angle of the intrinsic vector.
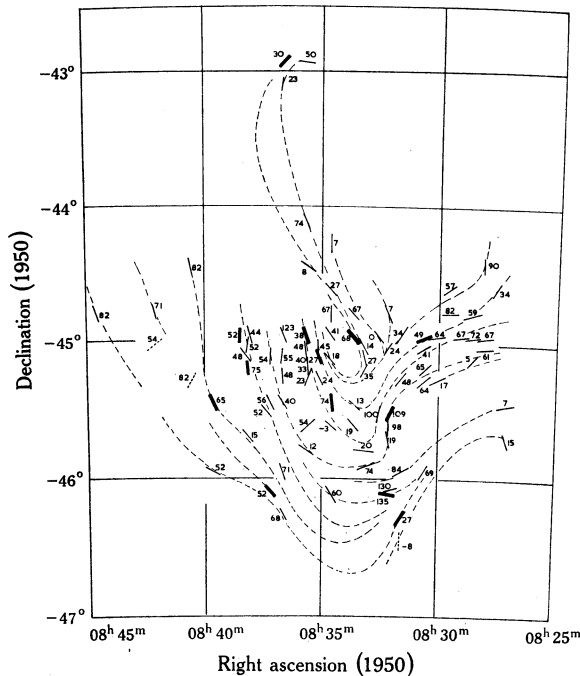

Fig. 6.—Direction of the transverse component of magnetic field in the Vela complex. The vectors shown have direction only; the magnitude of the field is not known at any point. The thickness of each vector is an indication of the reliability of the determination of direction at that point. The magnetic field suggested by these directions has been sketched in (the interpretation is discussed in the text). The number beside each vector is the rotation measure at that point (rad m^{-2}).

Magnetic field directions, orthogonal to the intrinsic polarization, are displayed in Figure 6. This figure also shows the rotation measure at each point where the magnetic field direction has been obtained. A magnetic field directed down the eastern side of the source, through Vela-X, and up the western side is a possible interpretation (sketched in Fig. 6). Certainly there is some evidence of a general circumferential field plus a more complicated field in the inner region. The low percentage polarization on the brighter parts of Vela-X may indicate that the field is directed along the line of sight at this point, lowering the intrinsic polarization and increasing the depolarization due to Faraday rotation effects. The picture is very complicated near the peak of Vela-X, with the rotation measure changing from its lowest value to almost its highest in the space of less than one-quarter of a degree.

It is possible to deduce something about the line-of-sight component of the magnetic field in the source. If it is assumed that Faraday rotation occurs in the source itself and that the field directions taken over the entire source are symmetrical in the line of sight, then the average rotation measure ($+46$ rad m^{-2}) would represent the rotation in the interstellar medium between the Sun and the source. Those parts

of the source exhibiting a rotation measure greater than $+46$ rad m^{-2} would have a line-of-sight magnetic field component directed towards the observer. A magnetic field away from the observer is implied by rotation measures less than $+46$ rad m^{-2}. An interstellar rotation measure of $+46$ rad m^{-2} is acceptable in this direction, where we are looking almost directly along the galactic magnetic field (Gardner and Whiteoak 1966). With an assumed distance of 500 pc this rotation measure would require an electron density by magnetic field product of 10^{-7} G cm^{-3}, say an average electron density of $0\cdot02$ cm^{-3} with a magnetic field of 5×10^{-6} G, acceptable values for these parameters. It does seem that the regions of highest percentage polarization avoid those areas where the rotation measure has extreme values (both high and low). This is to be expected if these extreme values are located where the magnetic field in the source is directed along the line of sight.

The integrated polarization of the whole source is of interest for comparison with the polarization of other, unresolved sources. The 2650 MHz electric vectors distributed over the source were added vectorially and combined with the integrated brightness of the source. This gave 109° and less than 1% for the position angle and percentage polarization respectively. The integrated brightness temperature of the source is 90°K at 2650 MHz. The low percentage polarization of the source if seen unresolved is an indication of the complexity or random nature of the source compared with many of the extragalactic objects (Gardner and Davies 1966). It may explain why polarization has been detected only weakly in the other smaller and less intense supernova remnants.

Depolarization of the polarized emission follows the most commonly occurring trend, i.e. decreasing percentage polarization with decreasing frequency. The depolarization over the region expressed as a parameter, the polarization ratio, has been calculated where possible (and listed in Table 2). This ratio, which is the ratio of percentage polarization at 2650 MHz to that at 1410 MHz, varies from 1 to 11 over the region, with a mean value of about 3. There appears to be no correlation between the polarization ratio and any other parameter. In particular no correlation was found with rotation measure, which might be expected if the rotation or part of it occurred within the emitting region. There is evidence of considerable beamwidth effect in the distribution of depolarization. This is to be expected in a source of this nature, and it further complicates any deductions from the depolarization data.

V. Optical–Radio Comparison

Observationally there is a strong resemblance between the distribution of radio emission and optical features for most optically unobscured supernova remnants, e.g. the Cygnus loop (Harris 1962) and IC 443 (Hogg 1964). This agreement is contrary to what one would expect with two different emission mechanisms operating, if they are sufficiently independent. Optically the objects are bright only in line emission, whilst at radio frequencies the distribution often contains an intense nonthermal source or sources, which derive their emission from the motion of high energy electrons in relatively strong magnetic fields. One does, however, expect that the optical filaments and the more widely distributed but lower density ionized

hydrogen would be seen as thermal emission at the shortest radio wavelengths. In the Vela complex the agreement between the general outline on Hα light and the weaker 2650 MHz contours (Fig. 7) is good. The strongest radio emission does, however, come from a region devoid of optical emission and where optical absorption does not seem excessively high. A minimum in the radio emission, at all frequencies, is centred on R.A. $08^h 35^m$, Dec. $-43° 30'$ and has its optical counterpart in the dark patch bounded rather abruptly by the northern arcs and the shells to the west. At 2650 MHz general agreement is evident in the boundary up the eastern face and the shells that form the western side of the nebula, but at lower frequencies (e.g. see Fig. 1(b)) the radio emission extends more eastward of this eastern face.
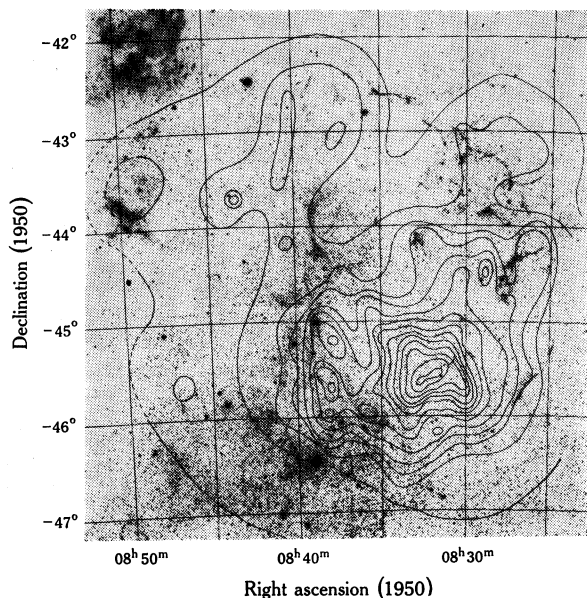
Fig. 7.—A mosaic, made from four 26 in. Schmidt plates, taken in Hα light showing the Stromlo 16 nebula overlaid with the 2650 MHz isotherms of Figure 1(d). The mosaic has been reproduced from Milne (1968).

In other words, there is an essentially nonthermal region beyond the boundary of the thermal radio emission and Hα emission. This has already been noted in the steepening of the radio spectrum near Vela-Y and Z (Section III). The faint Hα emission that forms the eastern face of Stromlo 16 is not easily discernible on published plates of the region and it has been assumed that the nebula had circular symmetry with obscuration over the eastern half. As has been pointed out above, the thermal radio emission does not in fact extend eastward of the optical features. We interpret this as a D-shaped nebula possibly formed by non-uniform radial expansion.

A lower expansion of the nebula in the easterly direction would suggest that interstellar density in this region is substantially higher than around other portions of the nebula. It can be established by inspection of Figure 7 that higher absorption does exist to the east of R.A. $08^h 46^m$ and an estimate of its magnitude has been made from the colours and magnitude of OB stars in this direction (Velghe 1963). In Figure 8 is plotted the colour excess E_{B-V} against the distance modulus $m_0 - M_v$ for Velghe's stars west of R.A. $08^h 45^m$ and those east of R.A. $08^h 48^m$. An absorption of $0·6$ mag/kpc is indicated in the former region with an additional $1·5$ mag/kpc in

the latter region. It is not completely clear where this additional absorption takes place, although a maximum distance of 500 ± 100 pc ($m_0-M_v = 8^m$ to 9^m) is suggested from Figure 8. It is possible that this absorption is the western extremity of the Vela dark cloud, which Greenstein (1937) estimates to be at a distance of between 500 and 750 pc.
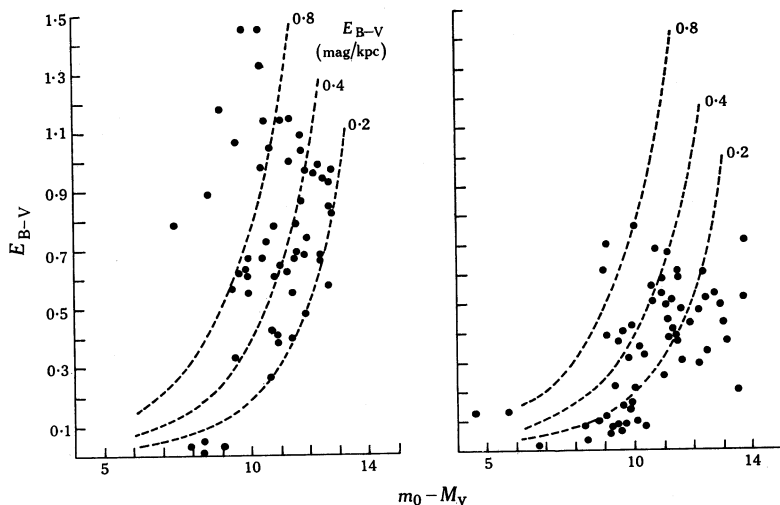

Fig. 8.—Diagram of colour excess E_{B-V} versus distance modulus m_0-M_v for the OB stars measured by Velghe (1963) in the region (a) east of R.A. $08^h 48^m$ and (b) west of R.A. $08^h 45^m$ (covering Stromlo 16). The increased absorption on the eastern side of Stromlo 16 is evident. .

VI. DISTANCE TO THE NEBULA

Harris (1962) suggested two distances for Vela-X: 700 pc from the angular size of the filaments in the nebula and 460 pc from Shklovsky's relationship between the surface brightness and radius of an expanding synchrotron emitter. The validity of the first of these methods has not been adequately demonstrated. Observations confirming Harris's findings have not been made and our understanding of the physics of filament formation still does not provide a basis for a constancy of filament size, object to object. The second method (Shklovsky's) considers the source as a filled spherical synchrotron emitter, whilst it is indicated here that Vela-X may have a shell structure and that part of the radio emission is certainly thermal (see Section VII).

The similarities between Vela-X, IC 443, and the Cygnus loop have been noted. The Cygnus loop has a well-determined distance of 770 pc (Harris 1962) and IC 443 has a probable distance of 2000 pc, although hydrogen line absorption indicates that IC 443 could be as close as 800 pc (Hogg 1964). Taking the angular diameters of the Cygnus loop and IC 443 to be 170′ and 45′ (Harris 1962) then with a diameter of 4° for Vela-X we would, by analogy with the Cygnus loop, expect it to be at a distance of 540 pc. The analogy with IC 443 (at 2000 pc) would indicate a distance of 375 pc.

If Vela-X is associated with the Vela dark nebula, as has been suggested in Section V, the distance would lie between 500 and 750 pc, following Greenstein's (1937) estimate for the distance to the absorption. We will adopt a value of 500 pc giving a diameter of 35 pc.

VII. THERMAL RADIO EMISSION AND ELECTRON TEMPERATURE

Johnson (1960) gives contours of surface brightness for the Stromlo 16 region in Plate 7 of his absolute isophotometric survey of the Milky Way. The correlation between his $\lambda6560$ Å (passband 326 Å) and the author's Hα plates is good in form and brightness. The comparison isophotes in the band at $\lambda6070$ Å are, however, inconsistent, and so Johnson's method could not be used to obtain the emission measure of the region. A background brightness of $1 \cdot 5 \times 10^{-4}$ erg sr^{-1} cm^{-2} sec^{-1} in the passband at $\lambda6560$ Å was therefore adopted and the isophotes, above this level, were integrated over the region occupied by the radio source to give an
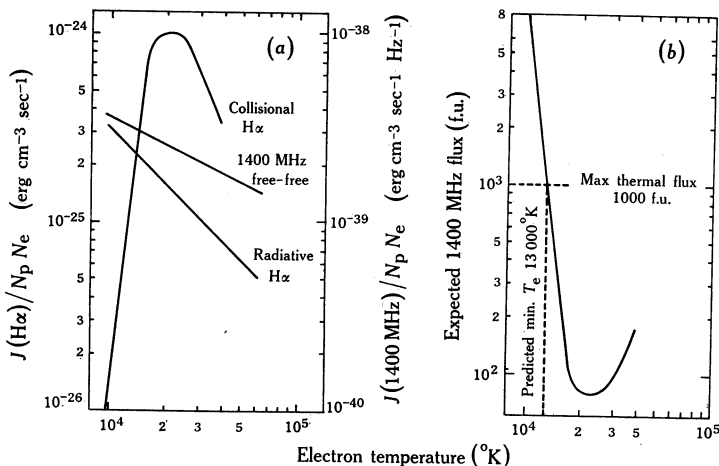

Fig. 9.—Plots as a function of electron temperature of (a) volume emissivities at 1400 MHz and in the Hα line for collisional and radiatively excited models, and (b) 1400 MHz flux expected from the measured Hα flux (3×10^{-7} erg cm^{-2} sec^{-1}); (b) is based on a collisionally excited model optically thick in the Lyman lines and optically thin in the Hα line and at 1400 MHz. The total flux at the highest frequency indicates, as described in the text, a lower limit to the electron temperature.

approximation for the free–free radio emission expected from the region. A flux at $\lambda6560$ Å of $4 \cdot 7 \times 10^{-7}$ erg cm^{-2} sec^{-1} was obtained from this integration. A large fraction of this may be due to the [N11] $\lambda6583$ and 6548 Å contribution, which could be easily as high as the Hα intensity if much of the gas is collisionally excited (e.g. see Milne 1968, Fig. 3). Allowing for this, and for 0·3 magnitude of absorption (i.e. average of 0·6 mag/kpc (Section V) and a distance of 500 pc), a final estimated Hα flux of about 3×10^{-7} erg cm^{-2} sec^{-1} was obtained.

We can relate this Hα flux to the radio frequency free–free emission if the excitation process populating the third quantum level of the hydrogen atom is

known. Provided the nebula is optically thin in both the $H\alpha$ line and at the radio frequency then the ratio of the fluxes $S_{\mathrm{r.f.}}/S_{H\alpha}$ is simply the ratio of the volume emissivities $j_{\mathrm{r.f.}}/j_{H\alpha}$ of the radio frequency and in the $H\alpha$ line. Figure 9(a) gives the volume emissivities at 1400 MHz (Oster 1961) and in the $H\alpha$ line, the latter for collisional excitation (Parker 1964a) and for radiative excitation (Burgess 1958) when the nebula is optically thick in the Lyman lines in both these cases.

Using the data of Figure 9(a) and the $H\alpha$ flux (3×10^{-7} erg cm^{-2} sec^{-1}) estimates have been made of the 1400 MHz radio flux that would obtain from Stromlo 16 if it were a collisionally excited nebula. This is displayed as a function of electron temperature T_e in Figure 9(b). It is likely that Stromlo 16 is a collisionally excited region with an electron temperature of between 10^4 and 2×10^4 °K, the range suggested from optical measurements made on filaments in the region (Milne 1968) and near those obtained by Parker (1964b) for other supernova remnants. It is unfortunate that $H\alpha$ volume emissivity, for a collisionally excited nebula, is a steep function of temperature below 20 000°K; we can therefore say very little about the magnitude of the expected free–free radio flux. However, from the radio spectrum of the source (Fig. 5) we expect that the optically thin thermal radio flux is less than 1000 f.u., which from Figure 9(b) would impose a lower electron temperature limit of about 13 000°K on the nebula. The minima in the collisional function near $T_e = 20 000$°K (Fig. 9(b)) requires that the free–free radio flux is at least 70 f.u., i.e. about 5% of the total 1410 MHz flux.

Dr. Whiteoak (personal communication) has suggested that the above allowance for absorption might be inadequate, particularly with recent determinations of the absorption-to-reddening ratio. An increase in the absorption, say by a factor of 2, to $0^m\cdot6$ would displace the curve of Figure 9(b) upward by a factor of $1\cdot3$. Because of the steepness of this curve the predicted minimum temperature would rise only by a small factor to a little less than 14 000°K.

VIII. MASS OF THE NEBULA

We can make estimates of the "visible" mass of Vela-X from either the $H\alpha$ flux or the free–free radio flux. However, unless we know the electron temperature more accurately estimates made from the former measure will contain an uncertainty of the order of 100, as will estimates made from the limits of free–free radio flux discussed in Section VII. Until a more reliable temperature can be used or an estimate of the free–free flux is made (i.e. from higher frequency measurements) we can only place limits on the visible mass of the nebula.

Assuming a distance of 500 ± 100 pc to Vela-X and adopting an average electron density of 300 ± 100 cm^{-3} (Westerlund 1966), we arrive at limiting hydrogen masses of $0\cdot05$ and $4M_\odot$ from the limits on the free–free radio flux discussed in Section VII (i.e. 70 and 1000 f.u.). For this determination a free–free volume emissivity of $3\times10^{-39} N_e N_p$ erg cm^{-3} sec^{-1} Hz^{-1} was used. This assumes a temperature of about 15 000°K (the free–free emissivity is only dependent on the square root of the temperature).

A further estimate of the mass may be made by considering how much mass has been swept up by the nebula expanding into an ambient interstellar gas density

of say $0 \cdot 1$ hydrogen atoms cm^{-3}. Once again assuming a distance of 500 ± 100 pc, and taking an average diameter between $3° \cdot 5$ and $4° \cdot 5$, we estimate this mass to be between 30 and $170 M_\odot$. These mass estimates are similar to Parker's (1964b) values for the Cygnus loop, for which the complete mass is believed to be about $100 M_\odot$. Parker has suggested that this higher mass could be responsible for the observed Hα flux if the temperature is lowered to 10 000°K. (This, however, would then not produce the observed forbidden spectra.) A similar argument applies to Vela-X, but in this case the excessively high radio emission produced would rule out the lower temperature—this, of course, is the basis of the upper limit imposed on the mass in this section.

IX. Conclusions

Summing up, it would appear from the brightness distributions shown here that Vela-X, Y, and Z comprise one source having a bright nonthermal component on the southern side (Vela-X) with substantial thermal emission, mainly to the north of Vela-X. The shape is reminiscent of certain other remnants having an annular brightness distribution (suggestive of shell structure) with one or two very bright regions on this distribution.

The radio polarization is stronger in the Vela complex than is usually found in supernova remnants. Some explanation for this may lie in the high effective resolution that we have as a consequence of the large angular size of this source. With this large angular size we have been able to obtain a fairly clear idea of the projected direction of the magnetic field over the object. However, without knowing with certainty the line-of-sight component of field it is difficult to establish a model for the magnetic field distribution. A circumferential field is a possible deduction from the data.

It has been proposed that the nebula is prevented from expanding on the eastern side by the presence of dense interstellar material, and it is suggested here that this would lead to a distance of about 500 pc. A comparison of the Hα flux and the radio flux leads to a possible minimum electron kinetic temperature of 13 000°K.

X. Acknowledgments

XI. References

Burgess, A. (1958).—*Mon. Not. R. astr. Soc.* **118**, 477.
Cooper, B. F. C., Cousins, T. E., and Gruner, L. (1964).—*Proc. Instn Radio Engrs Aust.* **25**, 221.
Gardner, F. F., and Davies, R. D. (1966).—*Aust. J. Phys.* **19**, 441.
Gardner, F. F., and Milne, D. K. (1963).—*Proc. Instn Radio Engrs Aust.* **24**, 127.
Gardner, F. F., and Whiteoak, J. B. (1962).—*Phys. Rev.* **9**, 197.
Gardner, F. F., and Whiteoak, J. B. (1966).—*A. Rev. Astr. Astrophys.* **4**, 245.
Greenstein, J. L. (1937).—*Ann. Harv. Coll. Obs.* **105**, 359.
Gum, C. S. (1955).—*Mem. R. astr. Soc.* **67**, 155.
Harris, D. E. (1962).—*Astrophys. J.* **135**, 661.

HILL, E. R., SLEE, O. B., and MILLS, B. Y. (1958).—*Aust. J. Phys.* **11**, 530.

HOGG, D. E. (1964).—*Astrophys. J.* **140**, 992.

JOHNSON, H. M. (1960).—Memoir No. 15, Mt. Stromlo Observatory.

MACKEY, M. B. (1964).—*Proc. Instn Radio Engrs Aust.* **25**, 515.

MATHEWSON, D. S., HEALEY, J. R., and ROME, J. M. (1962).—*Aust. J. Phys.* **15**, 354.

MILNE, D. K. (1966).—Symp. on Radio and Optical Studies of the Galaxy, Mt. Stromlo, p. 74.

MILNE, D. K. (1968).—The optical spectrum of Vela-X. *Aust. J. Phys.* **21** (in press).

OSTER, L. (1961).—*Astrophys. J.* **134**, 1010.

PARKER, R. A. R. (1964a).—*Astrophys. J.* **139**, 208.

PARKER, R. A. R. (1964b).—*Astrophys. J.* **139**, 493.

PIDDINGTON, J. H., and TRENT, G. H. (1956).—*Aust. J. Phys.* **9**, 481.

RISHBETH, H. (1958).—*Aust. J. Phys.* **11**, 550.

VELGHE, A. G. (1963).—Preprint, Royal Obs. of Belgium.

WESTERLUND, B. (1966).—*In* Discussion following Milne (1966), Symp. on Radio and Optical Studies of the Galaxy, Mt. Stromlo, p. 77.

WILSON, R. W., and BOLTON, J. G. (1960).—*Publs astr. Soc. Pacif.* **72**, 331.